Comparison of μ_2-scaled Hückel theory and Hartree–Fock theory of boranes and carboranes

Roger Rousseau and Stephen Lee[a)]
Department of Chemistry, The University of Michigan, Ann Arbor, Michigan 48109-1055

(Received 19 May 1994; accepted 15 September 1994)

The μ_2-scaled Hückel method is used to calculate the electronic energy surfaces of the four boranes $B_nH_n^{2-}$ ($n=8-11$) and the carborane $C_2B_8H_{10}^{2-}$. These electronic energy surfaces and their minimum energy geometries are directly compared to both the single crystal x-ray determined structures and to Hartree–Fock optimized geometries. Bond distances differ on the average by 0.04 Å between alternate methods. It is shown that μ_2-scaled Hückel results may be directly interpreted by analysis of the highest occupied and lowest unoccupied molecular orbitals. Also studied by the μ_2-scaled Hückel and Hartree–Fock methods are the isomerization pathways of $B_8H_8^{2-}$, $B_{11}H_{11}^{2-}$, and $C_2B_8H_{10}^{2-}$. Reaction barriers and transition state geometries found by the two different calculational methods are in fair agreement with each other and known literature values. Using the μ_2-scaled Hückel method one can readily deduce that the $B_8H_8^{2-}$ and $B_{11}H_{11}^{2-}$ isomerizations are Woodward–Hoffmann allowed reactions. In the case of $B_8H_8^{2-}$ this allowed mechanism is contrasted to an alternate Woodward–Hoffmann forbidden pathway. Hartree–Fock calculations on the $C_2B_8H_{10}^{2-}$ confirm earlier μ_2-scaled Hückel based findings, that a second less stable isomer of $C_2B_8H_{10}^{2-}$ exists which, in contradiction to Wade's rules of electron deficient clusters, has a pair of open square faces in the cluster. © *1994 American Institute of Physics.*

I. INTRODUCTION

There are two general approaches in the study of the electronic structure of molecules or solids. On the one hand, there are *ab initio* methods, such as the density-functional or Hartree–Fock theories which try to accurately assess all contributions to the electronic energy and thus give a numerically correct account of the total energy.[1] On the other hand, there are model calculations such as the pair potential or the extended Hückel method which try to find leading factors responsible for molecular stability and study the evolution of these factors among different structures.[2] Today the *ab initio* methods are primarily used for smaller systems, containing up to several hundred electrons in the molecule or unit cell, while the computationally faster model methods are applied to larger systems containing up to several hundred atoms in the molecule or unit cell.

The differences between *ab initio* and model methods extend however beyond the sizes of the systems treated. These differences may be summarized as follows. In the main, *ab initio* calculations produce reliable numbers useful in differentiating the often minute differences in energies of alternative structures. Excellent reviews of the accuracy of the *ab initio* methods are given in Ref. 1. By contrast, model calculations produce models useful in explaining these differences in energy. Well-known examples of these model concepts are the isolobal analogy, the conservation of orbital symmetry, and the concept of frontier orbitals.[2]

This division between these two schools of calculation is unsatisfactory. On the one hand, a calculational method which provides reliable energies, but few conceptual insights into the provenance of these energies is more of a computational method than a full fledged theory. On the other hand, a method which provides insights but not reliable energies can be accused of sureality.

In the past few years we have used a variant of Hückel theory, involving scaling of the second moment of the electronic density of states to produce reliable estimates of structural stability.[3] Unlike unscaled Hückel theory, these estimates are based directly on the calculated total electronic energies of the structures under study. This method is effective when the bonds being formed or broken are between atoms of the same kind. Thus the method works well with covalent or metallic bonds as opposed to ionic bonds. We have shown that second moment scaled Hamiltonians can account for electron-counting rules such as Wade's rules for electron deficient clusters,[4] the Hume–Rothery rules for noble and transition metal alloys,[5] and the octet rule of main group compounds. We have further used this method to produce optimal energy structures for both solids and molecules that are in reasonable agreement with experiment. Systems studied include solids[6] such as elemental boron, zinc, gallium, manganese, $LaSe_2$, $La_{10}Se_{19}$, and $RbDy_3Se_8$ and molecules such as boranes, carboranes, simple hydrocarbons, phosphorus–sulfur clusters, and transition metal carbonyl clusters. To date we have used this method in the rationalization of stable molecular or solid state geometries. Heretofore, we have neither studied the shape of the electronic energy surface nor the problem of chemical reaction pathways.

In this paper we address these latter issues while studying borane and carborane clusters. As we cannot directly compare electronic surfaces to easily accessible experimental data, we compare our electronic surfaces to those produced by Hartree–Fock theory. We then study the rearrangement pathways found in borane and carborane clusters. Here we compare results of second moment scaled Hückel theory to both NMR data and Hartree–Fock calculations. We find that for homoatomic systems the energies of the second moment

[a)]Author to whom all correspondence should be addressed.

 0021-9606/94/101(12)/10753/13/$6.00

scaled approach are in substantial agreement with those from moderately large basis set Hartree–Fock calculations. Further, the results of the second moment scaled Hückel theory may be directly explained through model concepts such as the Woodward–Hoffmann rules. We therefore hope that these results will aid in bridging the gap between *ab initio* and model calculations. Our results certainly affirm the continued pertinence of concepts such as HOMO–LUMO (highest-occupied–lowest unoccupied molecular orbitals) interactions, frontier orbitals, and the conservation of orbital symmetry in electronic structure theory.

II. CALCULATIONAL METHOD

A well-known error of extended Hückel (eH) and other tight-binding theories is their insufficient estimate of the repulsive energy between atoms. For example, in a molecule such as H_2 the extended Hückel or Hückel electronic energy is optimized when the two hydrogen nuclei fuse into a single nuclear core. The extended Hückel method therefore relies heavily on the insights that the shapes of the molecular orbitals provide us about the nature of the chemical bond. When coordination number and bond distances are kept constant however, the differences in Hückel or eH energies between structural alternatives can correspond well with observed structural data.[7] For example, Hückel theory is able to account for the linear or bent geometries found in AB_2 systems[3(b)] (where both A and B are main group atoms). The fact that differences in energies are useful in these latter systems can be correlated to the aforementioned repulsive energy error in the Hückel method. In particular, repulsive energy is a short-ranged interaction. One can therefore assume that repulsive energy is a function only of nearest-neighbor interactions and is therefore proportional to coordination number. In problems where coordination number and bond lengths are kept constant, repulsive energy is therefore constant and thus differences in energies between structural alternatives need not account for the repulsive energy.

That differences in Hückel energy are reasonable when bond distances are constant shows that the tight binding methods provide a fair representation of the electronic surface for dimensionless variables such as bond angles. For a system controlled by N different geometrical parameters it is always possible to express $N-1$ parameters as dimensionless quantities, leaving only a single size dependent parameter. To improve the Hückel or eH method one therefore needs to find a correction factor for this single variable.

The relation between size and electronic energy is a well-studied problem, particularly so for diatomic systems, where size is the sole geometrical variable.[8] It is known empirically that the Morse potential provides a reasonable estimate for the electronic surface, where the Morse potential is

$$E_{\text{tot}}(r-r_0)=A(-2e^{-\beta(r-r_0)}+e^{-2\beta(r-r_0)}). \tag{1}$$

This potential divides the total energy into attractive and repulsive components where the attractive and repulsive energies both decay exponentially as a function of distance, the attractive part decaying with an exponential constant of $-\beta$ and the repulsive part with the exponential constant of -2β. These exponential decay factors bear a clear resemblance to the analytical forms of various integrals which arise in electronic structure theory.[9] Thus, for Slater type orbitals the overlap and kinetic energy integrals at large r have exponential constants of $-\beta'$ while electron–electron Coulombic integrals and electron–nuclear integrals decay exponentially with the constant $-2\beta'$. In Hückel theory, the electronic energy has only an attractive potential. This attractive potential depends only on the overlap integral which as we mentioned above has an exponential decay like that found for the pure kinetic energy. To fashion a Morse-like potential we therefore need to include a second repulsive energy term, which decays as the square of the overlap integral. We therefore propose that E_{tot}

$$E_{\text{tot}}(r)=E_{\text{Hü}}+\sum \gamma_{ij}(S_{ij})^2, \tag{2}$$

where $E_{\text{Hü}}$ is the Hückel energy of the system calculated from the Wolfsberg–Helmholz approximation[10] for off-diagonal matrix elements of the Hückel Hamiltonian, γ_{ij} are weighing factors, and $S_{ij}(r)$ are the overlap integrals for the atomic orbitals ϕ_i and ϕ_j. To convert Eq. (2) into a workable expression for the total energy we need to determine the values of γ_{ij}. To do so we recall that the repulsive energy, the second term in Eq. (2), is approximately proportional to coordination number. We therefore need to find coefficients γ_{ij} such that

$$\sum \gamma_{ij}(S_{ij})^2 \propto C, \tag{3}$$

where C is the coordination number.[11] There are a number of functions which obey this property. One of the simplest is $\Sigma E_i^2-\Sigma(H_{ii})^2$, where E_i are the Hückel molecular orbital energies. To see that this is so first observe that changes in E_i are proportional to overlap and that therefore $\Sigma E_i^2-\Sigma(H_{ii})^2$ is linear in the squares of the overlap integrals. We further observe

$$\sum_i E_i^2-\sum_i (H_{ii})^2=\text{Tr}(H^2)-\sum_i (H_{ii})^2=\sum_{i\neq j} H_{ij}H_{ji}. \tag{4}$$

In this last equation we use atomic orbitals as the basis set by which we express our Hamiltonian. This latter sum in effect counts the number of atomic orbitals ϕ_j which are in bonding contact with the orbital ϕ_i. This number is proportional to the coordination number. This proves that $\Sigma E_i^2-\Sigma(H_{ii})^2$ is proportional to the coordination number. We therefore can express E_{tot}

$$\begin{aligned} E_{\text{tot}}(r)&=E_{\text{Hü}}(r)+\gamma\left(\sum_i E_i^2(r)-\sum_i (H_{ii})^2\right)\\ &=E_{\text{Hü}}(r)+\gamma\mu_2(r)-B, \end{aligned} \tag{5}$$

where we define the second moment of the density of states $\mu_2(r)=\Sigma E_i^2(r)$ and $B=\gamma\Sigma(H_{ii})^2$. The first term on the right-hand side of Eq. (5) is the attractive energy, $V(r)$, while the second is the repulsive energy, $-U(r)$. As the H_{ii} values in tight-binding theory are invariant to changes in geometry we may drop the term B from Eq. (5) when comparing systems with the same atomic constituents.

We now follow the argument first discussed by Pettifor.[3(c)] We consider two systems which we label 1 and 2. The terms E_{tot1}, U_1, V_1, E_{tot2}, U_2, and V_2 refer to the various energies of these two systems. We wish to calculate ΔE, where $\Delta E = E_{tot1} - E_{tot2}$. It may be seen that,

$$\Delta E = U_1(r_{1eq}) - V_1(r_{1eq}) - U_2(r_{2eq}) + V_2(r_{2eq}), \tag{6}$$

where r_{1eq} and r_{2eq} refer to the respective equilibrium sizes of the two systems.

We use the fact that we are interested in equilibrium geometries in the following way. Note that at equilibrium to a first-order Taylor expansion in distance, $E_{tot}(r)$ is constant. Therefore,

$$U_2(r_{2eq}) - V_2(r_{2eq}) \approx U_2(r_{2eq}+d) - V_2(r_{2eq}+d). \tag{7}$$

In particular we choose a value for d such that $U_2(r_{2eq}+d) = U_1(r_{1eq})$.

We now find that

$$\Delta E = E_{1Hü}(r_{1eq}) - E_{2Hü}(r_{2eq}+d). \tag{8}$$

We determine the value of r_{1eq} from the true experimental size of system 1 and the value d from the equality

$$\sum E_{1i}^2(r_{1eq}) = \sum E_{2i}^2(r_{2eq}+d). \tag{9}$$

The expressions to the left and right of the equal sign are the second moments of the molecular orbital energies, μ_2. In particular Eqs. (6)–(8) state that the differences in energy between two structural alternatives can be calculated from knowledge of the molecular orbital energies alone. It should be noted that the approximation given in Eq. (7) breaks down if the deviation in the values of μ_2 become significant.

To calculate these molecular orbital energies we use a minimal valence basis set. The Hamiltonian diagonal elements equal the energies of the isolated atomic orbitals while off-diagonal elements are calculated using the Wolfsberg–Helmholz approximation,[10]

$$H_{ij} = \frac{K}{2} S_{ij}(H_{ii} + H_{jj}), \tag{10}$$

where K is a constant traditionally set at 1.75 and S_{ij} is the overlap integral between the ith and jth atomic orbitals. The values for the diagonal H_{ii} terms are taken from work of the Hoffmann group for extended Hückel calculations.[12] The S_{ij} integrals are based on Slater type orbitals (STO) with single or double zeta expansions. Again the values of the STO exponents, ζ, are taken in conformity with values used in extended Hückel theory. It is important to note that the standard literature values for extended Hückel parameters are quite close to Hartree–Fock calculations.[13] For example the extended Hückel parameters for boron are $H_{ii}(2s) = -15.2$ eV, $H_{ii}(2p) = -8.5$ eV, $\zeta(2s) = 1.3$, and $\zeta(2p) = 1.3$. These correspond to the atomic Hartree–Fock parameters which are $H_{ii}(2s) = -13.46$ eV, $H_{ii}(2p) = -8.43$ eV, $\zeta(2s) = 1.288$, and $\zeta(2p) = 1.211$. Except in the case of contracted valence orbitals (such as the d orbitals in Zn or the s orbitals in Tl) we do not adjust Hückel or tight-binding parameters to improve our fit to experiment. In particular, in the current work on boranes and carboranes we have made no alteration to the literature parameters for boron, carbon, or hydrogen.

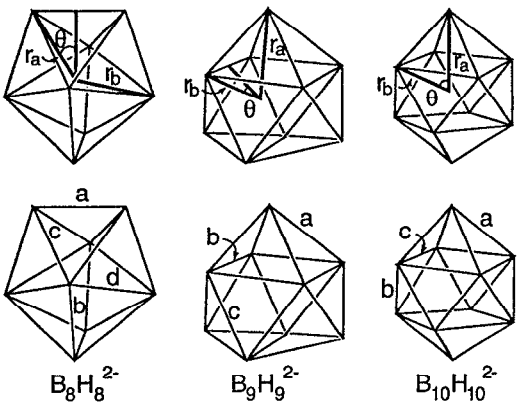

FIG. 1. The $B_8H_8^{2-}$, $B_9H_9^{2-}$, and $B_{10}H_{10}^{2-}$ clusters. Polyhedral vertices represent BH units.

In practice the second moment scaled calculations reduce to the following. When comparing two structural alternatives we calculate the molecular orbital energies of one of the structures at its true equilibrium size. For the second structure we scale its size so that its second moment exactly equals the second moment of the first. We then fill both molecular orbital diagrams with the requisite number of electrons and then calculate the difference in total electronic energies. We note that the constant γ remains undetermined in this procedure. We therefore study only the structural shape and not the overall volume dependence of the geometries in question. The chief advantage of this method of calculation is that it allows one to retain all the insights garnered from simple molecular orbital theory. This includes concepts such as the overlap of valence atomic orbitals, the HOMO–LUMO gap energy, the use of frontier orbitals, and finally the utility of minimal valence basis sets in determining molecular orbital energetics.

III. $B_nH_n^{2-}$ CLUSTERS

The structures of the boranes have been the subject of numerous studies and are well understood. It is now known that borane structures follow a set of principles generally referred to as Wade's rules for electron deficient clusters.[4] These rules state that $B_nH_n^{2-}$ dianions adopt a cluster geometry in which the boron atoms lie at the vertices of a purely triangular polyhedron. Each boron is bonded to just one hydrogen and these boron–hydrogen bonds point radially outward from the center of the polyhedron. The structures of three of these clusters ($B_8H_8^{2-}$, $B_9H_9^{2-}$, and $B_{10}H_{10}^{2-}$) are illustrated in Fig. 1.[14]

In earlier work we showed that second moment scaled Hückel theory can be used both to understand Wade's rules in general as well as to account for variations in specific boron–boron bond lengths.[3(f),3(i)] In our earlier work however, we did not consider other more traditional methods of electronic structure calculation. Such comparisons are important. Indeed with modern computing capabilities, one can

carry out much more rigorous *ab initio* Hartree–Fock calculations for these same systems.[15] This Hartree–Fock method is based on clear physical assumptions whose strengths and weaknesses are well catalogued.[1] For example, it is well known that Hartree–Fock theory generally produces correct ground state geometries as well as consistent vibrational spectra. A comparison of second moment scaled energies to Hartree–Fock values therefore allows one not just to assess the ability of second moment scaled theory to reproduce the global minimum geometry but also to study the shape of the electronic energy surface near this minimum.

In studying the electronic energy surface we are constrained by a number of factors. First, Hartree–Fock calculations are highly computer intensive.[16] Second, second moment scaled Hückel theory has several natural limitations. We have therefore restricted our study to just a few degrees of geometrical freedom. In particular, we consider dimensionless degrees of freedom which change neither the point group of the molecule nor the B–H bond distances. We consider only unitless degrees of freedom due to the breakdown of single determinantal theories (this includes both Hartree–Fock and Hückel theory) in correctly reproducing the electronic energy as a function of the overall size of the chemical system. We limit ourselves to variables which leave the point group symmetry of the molecule intact[17] as this not only drastically reduces the number of degrees of freedom but also because it is generally these geometrical variables which pose the greatest difficulty to traditional symmetry based molecular orbital analysis. Finally, we consider only distortions in the boron network, as second moment scaled theory is limited to distortions that do not result in excessive variable charge transfer. As the amount of charge transfer between the boron and hydrogen atoms depends on the boron–hydrogen bond distance, we keep such B–H distances constant.[18]

In Fig. 1 we illustrate the geometrical quantities used to define the pertinent degrees of freedom in $B_8H_8^{2-}$, $B_9H_9^{2-}$, and $B_{10}H_{10}^{2-}$. We consider first the $B_{10}H_{10}^{2-}$ molecule which has a D_{4d} ground state geometry. In $B_{10}H_{10}^{2-}$ there are two symmetry inequivalent types of boron atoms which lie at a distance either r_a or r_b away from the center of the cluster. The angle between r_a and r_b is defined to be θ. The boron positions in $B_{10}H_{10}^{2-}$ geometry are therefore controlled by three parameters: r_a, r_a/r_b, and θ. The first parameter is size dependent while the remaining two are dimensionless. As stated above we are interested only with the latter parameters. In a similar manner $B_8H_8^{2-}$ and $B_9H_9^{2-}$ have, respectively, D_{2d} and D_{3h} symmetry and, respectively, three and two dimensionless boron positional parameters. We therefore optimized these parameters for these three molecules using both second moment scaled Hückel theory (μ_2 theory)[19] and restricted Hartree–Fock theory at the STO-3G, 3-21G, and 6-31G* levels.[1(a)] A comparison of some of these results is given in Table I. The results are tabulated for all the symmetry inequivalent B–B bond lengths, where the tabulated specific bond labels refer to those illustrated in Fig. 1. We also show in Table I the average experimental x-ray structure bond lengths for these bond types. In comparing these results we see that there is significant overall agreement between the

TABLE I. Comparison of RHF, μ_2-Hückel and x-ray crystal structure bond distances for $B_8H_8^{2-}$, $B_9H_9^{2-}$, and $B_{10}H_{10}^{2-}$.

Bond	Expt.	μ_2	6-31G*	STO-3G
$B_8H_8^{2-}$				
a	1.56 Å	1.55 Å	1.70 Å	1.61 Å
b	1.72	1.62	1.69	1.65
c	1.76	1.82	1.83	1.78
d	1.93	1.92	1.96	1.91
$B_9H_9^{2-}$				
a	1.71 Å	1.69 Å	1.72 Å	1.68 Å
b	1.84	1.80	1.83	1.81
c	1.90	1.97	1.98	1.91
$B_{10}H_{10}^{2-}$				
a	1.68 Å	1.65 Å	1.70 Å	1.67 Å
b	1.79	1.78	1.83	1.79
c	1.82	1.87	1.85	1.83

μ_2 theory, the Hartree–Fock calculations, and the x-ray crystal structure distances. The average difference in bond distances between the RHF/6-31G* calculation and the experimental bond distances is 0.044 Å while the corresponding difference between the μ_2 theory and experiment is 0.040 Å. In general the ordering of the bonds from shortest to longest is the same for the μ_2 theory, the Hartree–Fock calculations, and the x-ray structures. Finally it should be recalled that in our second moment scaling procedure, we have in effect fixed the overall size of the system. It is therefore the variation in the bond lengths which should be compared to the RHF and x-ray bond distances.

We now turn to the shape of the electronic surface of these three molecules near the minimum energy geometries. We show in Fig. 2 a contour map of the three surfaces using μ_2 and the RHF/6-31G* theory. For the sake of simplicity we consider only a two-dimensional surface for $B_8H_8^{2-}$. Both theoretical and experimental minima are shown in Fig. 2. It may be seen that there is fairly good agreement between the *ab initio* and the μ_2 electronic surfaces, with the best agreement found for $B_9H_9^{2-}$ and the worst for $B_8H_8^{2-}$. There are however several major differences between these results. First we should note that only the Hartree–Fock theory is based on exact approximations and therefore only for Hartree–Fock theory is it known, at least in principle, which additional effects (such as configuration interaction) need to be included. Second, it is easiest to rationalize the geometrical factors responsible for the shape of these curves within the context of μ_2 theory. This is so as we have a fairly large set of useful molecular orbital techniques including the fragment formalism and the concept of orbital mixing which can be used to explain μ_2-Hückel molecular orbital energies. These approaches are particularly useful in the context of Hückel theory as it is possible to evaluate the energy of a Hückel orbital without considering other occupied molecular orbitals (as one has to do with Hartree–Fock theory). Further, Hückel energies depend purely on the overlap of valence atomic orbitals. Such overlap can be deduced by visual inspection of the molecular orbital (MO) shape. Finally, in Hückel theory one does not need to calculate directly the

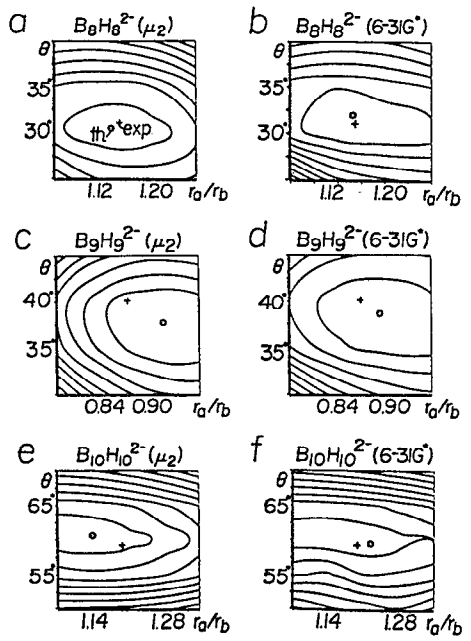

FIG. 2. Contour map of energy as a function of geometry for $B_8H_8^{2-}$, $B_9H_9^{2-}$, and $B_{10}H_{10}^{2-}$ from μ_2-Hückel and RHF 6-31G* calculations. Contour lines represent 0.05 a.u. Open circles and crosses represent calculated and experimentally observed minimum energy geometries respectively (see Fig. 1).

difference in energy between large nuclear–nuclear or electron–electron repulsions and large electron–nuclear attractions and one therefore obviates the need to explain small differences between large numbers. Thus in Hückel theory one can often reduce the difference in energy to the differences in energy of just a few key orbitals.

IV. THE θ PARAMETER OF $B_{10}H_{10}^{2-}$

The fragment formalism and the concept of orbital mixing can be used to account for the electronic energy surfaces of the borane dianions described in Sec. III. By way of illustration, in this section we consider in detail the $B_{10}H_{10}^{2-}$ ion. In the previous section (see Fig. 2) we saw that of the two dimensionless parameters in $B_{10}H_{10}^{2-}$ only the angle variable, θ, has a significant effect on the electronic energy. Indeed the minimum of the contour map in Fig. 2(c) has more the form of a trench than a local point minimum. The slopes of this trench correspond to changes in θ. We therefore concentrate here on this θ parameter. In Fig. 3 we have drawn a Walsh diagram for the individual MOs as a function of θ (where the remaining variable, r_a/r_b is held constant at the optimal value of 1.226). It may be seen that for $\theta=60°$ a large gap of MO energies appears between -13 and -5 eV. This corresponds to the HOMO–LUMO gap. The HOMO–LUMO gap is largest between 55° and 60° which agrees well with the optimized value of $\theta=60.8°$. However, it may be seen that changes of energy in the HOMO alone do not quantitatively account for the changes in total energy. The penultimate occupied molecular orbital (POMO) and other low lying orbitals also play significant roles. A good estimate of the relation

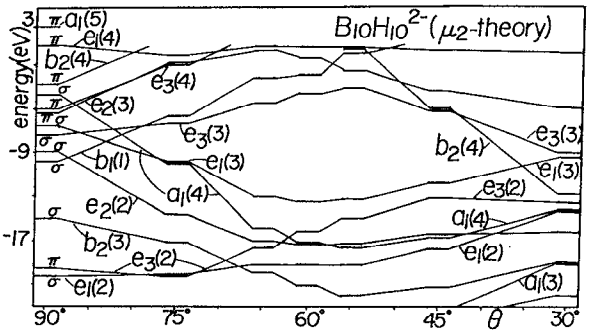

FIG. 3. μ_2-Hückel theory Walsh diagram for $B_{10}H_{10}^{2-}$ as a function of θ. (See Figs. 1 and 4.)

between energy and θ can be obtained if one analyzes the irreducible representation labels of the individual MOs. In particular, we consider the sum of the HOMO energies of each type of irreducible representations. As there are five types of filled MOs (the a_1, b_2, e_1, e_2, and e_3 representations of the D_{4d} point group) this sum consists of adding five separate MO energies together. In Table II we compare the energy of this sum with the sum of all filled MOs. In particular we calculate differences of energy between alternate structures using the $\theta=60°$ geometry as the reference standard. As Table II shows there is reasonable agreement with the two columns of energy differences. We therefore need to account for the energies of merely these five orbitals in deducing the relation between geometry and the overall energetics of the $B_{10}H_{10}^{2-}$ ion.

To do so we examine the evolution of the $B_{10}H_{10}^{2-}$ geometry as a function of θ. As is illustrated in Fig. 4, at $\theta=90°$ the molecule has a planar octagon of boron atoms sandwiched between two apical boron atoms. Of the three types of bonds illustrated in Fig. 1, the c bonds (which are the bonds in the two square planes of the $B_{10}H_{10}^{2-}$ molecule) have been entirely ruptured. By contrast, in the $\theta=30°$ regime the $B_{10}H_{10}^{2-}$ cluster has divided itself into two nearly isolated fragments, each of which separately has C_{4v} symmetry. With respect to Fig. 1, the bonds linking the two square faces, the b bonds, have been broken. The evolution of structure is clearly coupled to changes in the symmetry of the molecule. At $\theta=90°$ the point group symmetry is no longer D_{4d} but is rather of D_{8h} symmetry. This doubling in the number of

TABLE II. Comparison of ΔE sum for all MOs and sum of HOMOs of each irreducible representation for $B_{10}H_{10}^{2-}$.

θ	ΔE (all MO)[a]	ΔE (sum of HOMO)[b]
45°	22.6 (eV)	24.3 (eV)
55°	3.1	3.9
60°	0.0	0.0
65°	2.1	3.5
75°	21.6	31.6

[a]ΔE is the difference in energy between a given geometry and the $\theta=60°$ geometry. In the middle column we sum all filled MOs.
[b]In this column we sum the highest occupied molecular orbital energies of each of the a_1, b_2, e_1, e_2, and e_3 irreducible representations.

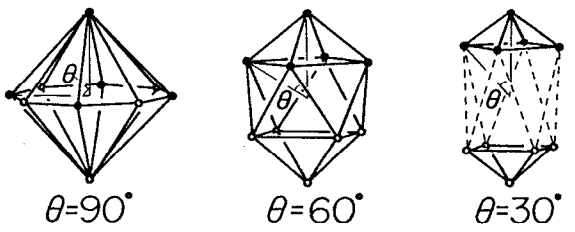

FIG. 4. Geometry deformation of $B_{10}H_{10}^{2-}$ as a function of θ. Open and closed circles represent the upper and lower B_5H_5 molecular fragments.

group elements, doubles the number of irreducible representations, with all orbitals being either symmetrical with respect to σ_h (the mirror plane which contains the planar octagon of boron atoms) or antisymmetrical with respect to this plane. In Fig. 3, we refer to these orbitals as having either σ (symmetric) or π (antisymmetric) symmetry. In a similar fashion there is an increase in symmetry at $\theta=30°$. At this angle there are two nearly dissociated $C_{4v}B_5H_5$ clusters. All molecular orbitals on one fragment have therefore an identical twin at the same energy on the second fragment. Symmetry principals require that $D_{4d}e_1$ orbitals pair up with e_3 orbitals and a_1 orbitals pair up with b_2 orbitals.

We therefore can develop a classic Walsh argument showing how changes in symmetry at both $\theta=90°$ and $\theta=30°$ lead to orbital mixing. Clear instances of this mixing may be seen in Fig. 3. For example, at $\theta=90°$, the orbital $e_2(3)$ (i.e., the third to lowest energy e_3 orbital) is of π symmetry while the $e_2(2)$ orbital is of σ symmetry. By symmetry these orbitals cannot mix. Away from 90° the π and σ labels are no longer maintained and hence these orbitals do mix. The result of this mixing is that the occupied $e_2(2)$ orbital is stabilized and correspondingly the unoccupied $e_2(3)$ orbital is destabilized. We can also consider the $\theta=30°$ case near the limit of two isolated B_5H_5 fragments. We find here for example that the $a_1(4)$ and $b_2(4)$ orbitals are quite close in energy as required by symmetry. As θ increases however, the two $C_{4v}B_5H_5$ fragments become increasingly coupled. This coupling has the effect of stabilizing the filled $a_1(4)$ orbital and destabilizing the unfilled $b_2(4)$ orbital. A detailed analysis of all the orbitals shows that the effect of mixing can account for the overall shape of Fig. 3.[20]

In this paper however we consider an alternate method for accounting for the overall energetics of the $B_{10}H_{10}^{2-}$ system. Rather than relying solely on symmetry principles, we study here instead the actual shapes of the individual orbitals. In particular we use the principle of conservation of orbital shape which notes that the shapes of individual orbitals transform in an analytically continuous fashion as a function of geometric change. This principle does not require the detailed symmetry based analysis and therefore can be used in systems which do not have high point group symmetries. It is particularly direct as it discusses changes in the orbitals themselves. In Fig. 5, we draw the shapes of the highest occupied a_1, b_2, e_1, e_2, and e_3 orbitals at both $\theta=90°$ and $\theta=30°$. As noted earlier, these five orbitals alone can account

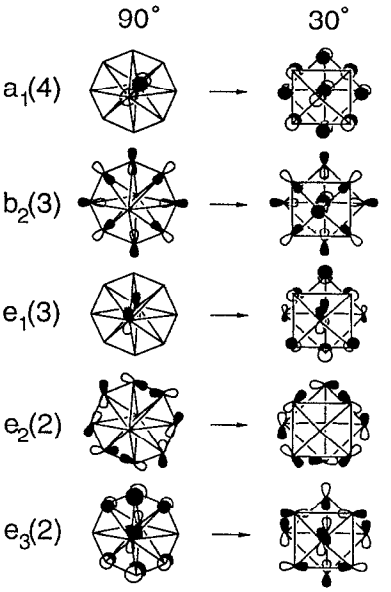

FIG. 5. The five highest molecular orbitals for the a_1, b_2, e_1, e_2, and e_3 irreducible representations of $B_{10}H_{10}^{2-}$.

for the energetics of the full $B_{10}H_{10}^{2-}$ system. As θ changes from 90° to 30° these orbitals transform continuously from those shown on the left of Fig. 5 to those on the right. This alternation is associated with the formation of the intrasquare c bonds and the simultaneous rupture of the intersquare b bonds. (See Fig. 1).

Among the five orbitals shown in Fig. 5, two of them, namely the $e_1(3)$ and $a_1(4)$ are arranged at $\theta=30°$ so that as the B_5H_5 fragments approach one another, strong intersquare b bonds may develop. This stabilization occurs only away from $\theta=30°$, as only at larger θ angles are there short enough B–B contacts to stabilize the overall system. As one approaches $\theta=90°$ however this overall stabilization energy is lost for the orbital character of these two orbitals is increasingly transferred into the apical boron atoms (see Fig. 5). Therefore the energies of both the $a_1(4)$ and $e_1(3)$ orbitals are parabolic functions of θ with a minimum between $\theta=30°$ and $\theta=90°$. This is directly confirmed by the full molecular orbital calculation shown in Fig. 3. The $b_2(3)$ and $e_2(2)$ orbitals shown in Fig. 5 both have strong intrasquare c bonds at $\theta=30°$. As θ increases these bonds are broken and replaced by, respectively, antibonding and weakly bonding intrasquare c bonds. Therefore both the $e_2(2)$ and $b_2(3)$ orbitals increase in energy as θ increases from 30° to 90°. This rise in energy is offset by the decrease in energy of the $e_3(2)$ orbital as θ increases over the same angle range. As Fig. 5 shows at $\theta=30°$ the $e_3(2)$ orbital is almost nonbonding while at $\theta=90°$ there are strong intersquare b bonds. The evolution from one regime to the other accounts for the sharp drop in the $e_3(2)$ orbital energy in going from $\theta=30°$ to $\theta=90°$. The net sum of these five orbitals gives an essentially parabolic shape to the total energy as a function of θ. This parabola has a minimum near the true global minimum of this system.

The above analysis shows that within the context of

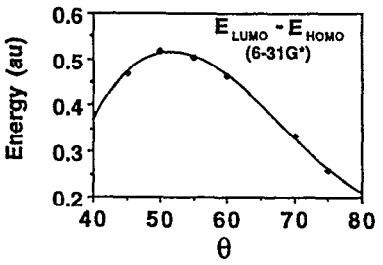

FIG. 6. RHF 6-31G* E_{elec} for $B_{10}H_{10}^{2-}$ as a function of θ.

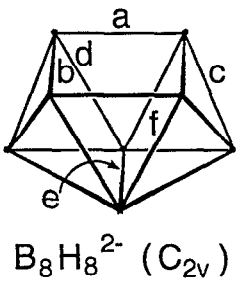

FIG. 7. Optimized C_{2v} geometry for $B_8H_8^{2-}$.

simple Hückel or tight-binding theory, concepts such as mixing of atomic orbitals, the importance of the highest lying occupied orbitals, and the principle of conservation of orbital symmetry and shape provide a powerful means of accounting for the overall electronic energy. We now consider the comparable analysis using Hartree–Fock theory. This theory differs from Hückel theory in several places. In the Hartree–Fock theory the electronic energy is not just the sum of filled molecular orbital energies.[1(c)] This is so as the molecular orbital energies, ϵ_i, in Hartree–Fock theory contain electron–electron repulsive energies. The sum ϵ_i actually double counts the electron–electron repulsive interactions. This difference between Hückel and Hartree–Fock molecular orbital energies has fundamental consequences. For example, in explaining the μ_2-Hückel results for $B_{10}H_{10}^{2-}$ we found that the HOMO–LUMO gap is largest near 60° and that this gap was due to mixing of HOMO and LUMO orbitals of the various different irreducible representations. This same explanation cannot be used to account for the Hartree–Fock results. In Fig. 6 we plot the HOMO–LUMO gap energy (for ϵ_i) for our RHF 6-31G* calculation. It may be seen that the Hartree–Fock HOMO–LUMO gap is largest at 51°. This differs significantly from the observed θ angle.[21] Hartree–Fock HOMO–LUMO gap energies are clearly not a reliable indicator of the $B_{10}H_{10}^{2-}$ equilibrium geometry. In fact, interpretation of the Hartree–Fock results is in many ways quite subtle. In Table III we show the sum of all molecular orbital energies for the RHF 6-31G* calculations as a function of θ. As these results indicate, it is difficult to directly deduce from the Hartree–Fock calculations the importance of the frontier orbitals to the stable conformation of a given chemical system. For example, the sum of all filled molecular orbital energies is actually a maximum at $\theta=60°$. Similarly the sum of the orbital energies which correspond to the highest occupied MOs of each irreducible representation type, while a minimum at $\theta=60°$, is a parabola with only a quarter of the curvature of the true E_{tot}. These difficult to interpret Hartree–Fock molecular orbitals energies are in strong contrast to μ_2-Hückel molecular orbital energies.

TABLE III. Comparison of Hartree–Fock 6-31G* energy terms[a] for $B_{10}H_{10}^{2-}$.

θ	ΔE_{tot}	$\Delta E(2\Sigma E_2)$[b]	$\Delta E(2\Sigma\text{HOMO})$[c]
45	27.3 (eV)	−22.6 (eV)	6.47 (eV)
50	11.1	−16.3	1.90
55	2.8	−11.8	0.54
60	0.0	0.0	0.0
65	2.1	−5.6	2.54
70	10.6	−7.5	6.64
75	28.2	−8.4	6.77

[a]All values reported are the differences in energy between a given geometry and the $\theta=60°$ geometry.
[b]In this column we sum the energies of all filled orbitals.
[c]In this column we sum the energies of the highest occupied orbitals of the a_1, b_2, e_1, e_2, and e_3 representations.

V. $B_8H_8^{2-}$ ISOMERIZATION

In the previous sections of this paper we examined the electronic energy surface near the equilibrium geometries of $B_8H_8^{2-}$, $B_9H_9^{2-}$, and $B_{10}H_{10}^{2-}$. We showed that μ_2-Hückel theory provided electronic energy surfaces near the global energy minimum that were in reasonable accord with *ab initio* theory. In this section we consider the energy surface away from the global minimum geometry. We examine here alternate local minima and the pathways which connect these local minima to the ground state global minimum. We turn first to the isomer chemistry of the molecule $B_8H_8^{2-}$ as well as the reaction pathways which connect these isomers. Again, we compare μ_2-Hückel theory with *ab initio* calculations at various levels (STO-3G, 3-21G, and 6-31G*). It should however be noted at the outset that both the *ab initio* and the μ_2 calculations will be less quantitatively accurate than the results of the preceding sections.

It is known that the $B_8H_8^{2-}$ ion in solution has only one ^{11}B NMR peak.[22] This single resonance is inconsistent with the two inequivalent boron sites found in the equilibrium D_{2d} structure found by x-ray single crystal studies. It is well established that there is a simple reaction mechanism which scrambles the boron atoms of $B_8H_8^{2-}$.[23] Several *ab initio* studies have suggested that a reasonable intermediate in this process is the C_{2v} geometry illustrated in Fig. 7.[24] We have therefore optimized the $B_8H_8^{2-}$ molecule in this C_{2v} geometry using μ_2 scaled-Hückel theory. We find that the optimized C_{2v} geometry is 7.2 kcal/mol higher in energy than the ground state D_{2d} geometry. This difference in energy may be compared to the 6-31G* and STO-3G energy which are found to be 0.85 and 4.5 kcal/mol, respectively. These results are similar to those based on an alternate self-consistent field method, the PRDDO approximation method, where the difference in energy was found to be 3.6 kcal/mol.[24(a)] The error between the μ_2-scaled energy and the

TABLE IV. Comparison of bond distances for $B_8H_8^{2-}$ in C_{2v} geometry.

Bond	μ_2-Hückel	6-31G*
a	2.048 (Å)	2.001 (Å)
b	1.688	1.684
c	1.871	1.855
d	1.644	1.688
e	1.884	1.826
f	1.848	1.764

6-31G* energy is therefore slightly greater than the error between different level basis set RHF calculations. The optimized bond distances of the 6-31G* and μ_2 Hückel calculations can be directly compared as is shown in Table IV. It may be seen that there is good agreement between the two theories.

We next consider the reaction pathway between the C_{2v} and D_{2d} minimum geometries. It is well established that the reaction coordinate which connects the D_{2d} to C_{2v} geometries is a diamond to square transition.[24] This is a transition in which a single bond between the common atoms of two adjacent triangular faces is broken thus fusing the two triangular faces into a single square face. In the case of $B_8H_8^{2-}$ it is known that the diamond to square transition is a Woodward–Hoffmann symmetry allowed mechanism. The pertinent diamond to square transition for $B_8H_8^{2-}$ is illustrated in Fig. 8. As this figure shows, the C_2 axis of the C_{2v} minimum is maintained throughout the reaction coordinate until finally becoming one of the two dihedral C_2 axes of the D_{2d} ground state minimum. Such a transition is reminiscent of the conserved C_2 symmetry operation in pericyclic rearrangements.[2(b)] Just as in pericyclic rearrangements it is possible to postulate other symmetry transformations between the reactant and product ground states. For example, a potential reaction coordinate is one in which the original S_4 axis of the D_{2d} minimum transforms into the C_2 axis of the C_{2v} minimum. Such a process is also illustrated in Fig. 8. As

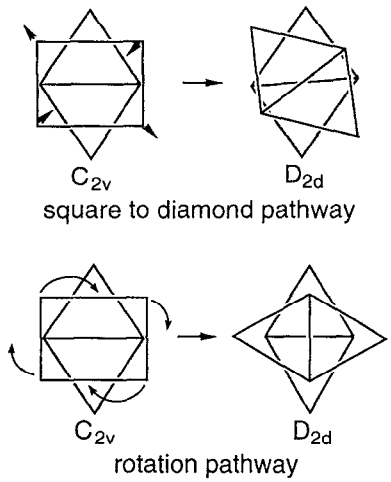

FIG. 8. The square to diamond and rotation pathways interconnecting the C_{2v} and D_{2d} isomers of $B_8H_8^{2-}$.

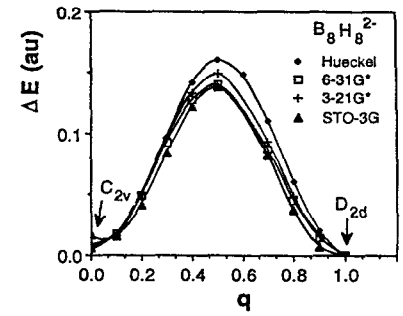

FIG. 9. Energy as a function of distortion coordinate, q, between the C_{2v} and D_{2d} isomers of $B_8H_8^{2-}$ along the rotation pathway.

Fig. 8 shows the former diamond–square transition involves a stretching of the initial square face of the C_{2v} geometry into a rhombus. The alternate mechanism in which the S_4 axis of the D_{2d} geometry becomes the C_2 axis of the C_{2v} geometry, has by contrast a 90° rotation in which the top square face rotates in the clockwise manner (see Fig. 8). We will therefore refer to the first mechanism as the diamond–square pathway and the latter as the rotation pathway. In analogy with the Woodward–Hoffmann analysis of pericyclic reactions we will now compare the energies of these two processes. In Fig. 9 we consider the rotation pathway, where we directly interpolate between the C_{2v} and D_{2d} minima. In Fig. 9 we compare the energy using the μ_2 scaled theory as well as at different levels of *ab initio* theory including the use of the STO-3G, 3-21G*, and 6-31G* basis sets. It may be seen that all levels of theory are in substantial agreement with a barrier height of 3 eV. This barrier is much too high to be the actual mode by which the boron atoms of $B_8H_8^{2-}$ isomerize in solution. In Fig. 10 we consider the diamond–square pathway between the C_{2v} and D_{2d} minima. We used here the method of hyperspheres[25] to calculate the reaction pathway. It may be seen that the transition state is only 0.3 kcal/mol higher in energy than the C_{2v} geometry. A similar low energy barrier is found at the *ab initio* level. At the

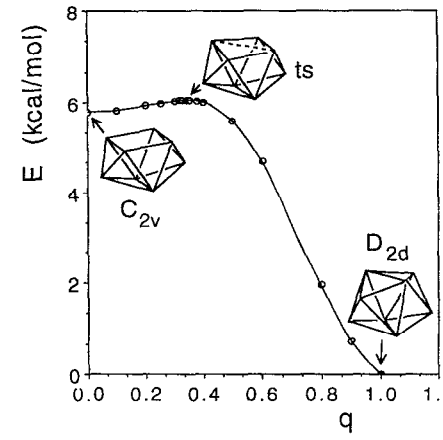

FIG. 10. Energy as a function of reaction coordinate along the square to diamond pathway for $B_8H_8^{2-}$.

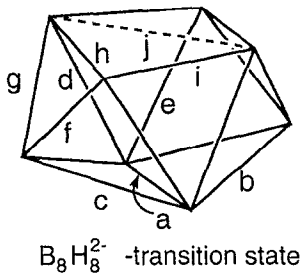

FIG. 11. The transition state between the C_{2v} and D_{2d} isomers of $B_8H_8^{2-}$.

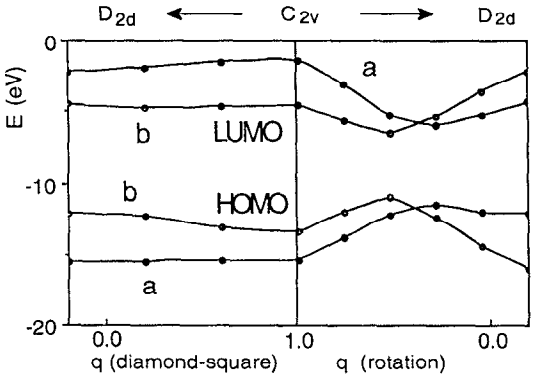

FIG. 12. Highest occupied and lowest unoccupied molecular orbital energies for the rotation and square to diamond pathways of $B_8H_8^{2-}$.

6-31G* level the difference in energy was less than 0.1 kcal/mol, while at higher levels of theory, the C_{2v} geometry was not a minimum.[24(d)] In Fig. 11 we illustrate the actual transition state geometry for the μ_2-Hückel theory. This transition state can be directly compared to the 6-31G* RHF transition state geometry. We compare the bond distances of the two transition states in Table V. As Table V shows, there is a close similarity between the transition states of the two different levels of theory. The substantial agreement between Hartree–Fock and Hückel theories implies that we can use either method to account for both the low transition state energy of the diamond–square mechanism and the high transition state energy of the rotation pathway. The Hückel method has the advantage over Hartree–Fock methods in that it is the actual sum of the occupied molecular orbital energies which equals the total electronic energy of the system. We can therefore turn to specific molecular orbital energies and state that it is the change in their energy which is responsible for the stability or lack of stability of a given geometry. We therefore turn to the Hückel HOMO and LUMO of the $B_8H_8^{2-}$ molecule along two pathways. We plot the energy of these orbitals in Fig. 12. This figure shows that there is a large increase in the HOMO energy along the rotation pathway. By contrast there is almost no increase in HOMO energy along the diamond–square pathway. Further the increase in the HOMO energy along the rotation pathway is roughly 3 eV, in substantial agreement with the total barrier height. It is therefore the change in HOMO energies which is responsible for the forbidden character of the rotation reaction pathway and the allowed character of the diamond–square pathway. We therefore need only to account for the changes in the HOMO energies. To do so we consider the actual shapes of these orbitals. These are illustrated in Fig. 13. It may be seen that the HOMO of the transition state is an interpolated average of the C_{2v} and D_{2d} HOMOs. The difference in the rotation and diamond–square pathways is that in the diamond–square transition state the HOMO is just as bonding as the C_{2v} or D_{2d} HOMOs. By contrast the rotation pathway HOMO is essentially nonbonding between the upper and lower four boron atoms shown in Fig. 13. It is therefore the conservation of orbital shape, and its resultant loss of HOMO bonding character which is responsible for the forbidden character of the rotation pathway.[26]

TABLE V. Comparison of $B_8H_8^{2-}$ transition state geometries.

Bond	μ_2-Hückel	RHF-6-31G* [a]
a	1.886 (Å)	1.837 (Å)
b	1.791	1.744
c	1.861	1.776
d	1.870	1.884
e	1.871	1.866
f	1.608	1.666
g	1.686	1.725
h	2.014	1.996
i	1.669	1.675
j	2.466	2.458

[a]Data taken from Ref. 24(d).

VI. $B_{11}H_{11}^{2-}$ AND $C_2B_8H_{10}^{2-}$ ISOMERIZATION

$B_{11}H_{11}^{2-}$ like $B_8H_8^{2-}$ has an interesting electronic energy surface. The ground state has C_{2v} symmetry. It is illustrated in Fig. 14. There are five symmetry inequivalent boron atom types in this structure. In solution however the ^{11}B NMR peaks have fused into a single line, indicating that the molecule is fluxional.[27] It is well established that the mechanism

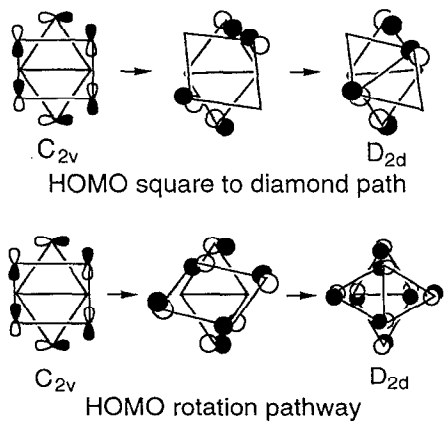

FIG. 13. Evolution of C_{2v} HOMO along the rotation and square to diamond pathways. Note that as shown in Fig. 12, the C_{2v} HOMO transforms into the POMO (penultimate occupied MO) or the D_{2d} HOMO along the respective pathways. For the sake of clarity we illustrate only the principal p components of each molecular orbital.

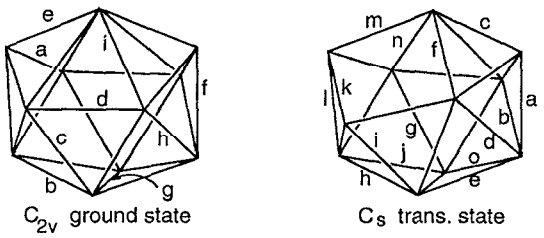

FIG. 14. The C_{2v} ground state and the C_s transition state geometries for $B_{11}H_{11}^{2-}$.

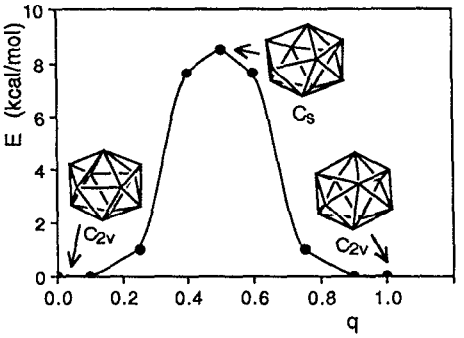

FIG. 16. Energy as a function of the dsd reaction coordinate for $B_{11}H_{11}^{2-}$.

of boron atom scrambling involves a diamond to square to diamond transition (dsd).[28] This scrambling mechanism is illustrated in Fig. 15. This dsd transition is of low symmetry. Both the mirror planes and the original C_2 axis of the ground state are destroyed in the dsd interconversion. The transition state itself is the only other point along the reaction pathway where there is a nontrivial symmetry element. The transition state is of C_s symmetry due to a mirror plane which bisects the open square face along its edges. Thus the dsd pathway involves a $C_{2v} \rightarrow C_1 \rightarrow C_s \rightarrow C_1 \rightarrow C_{2v}$ sequence of point group symmetries. At general positions along this reaction coordinate there are 27 independent geometrical degrees of freedom. Due to the large number of variables, we limited ourselves to the μ_2-scaled Hückel Hamiltonian for calculating the boron coordinates at general positions of the reaction coordinate. However for the higher symmetry ground state and transition state we carried out RHF calculations. In Fig. 16 we show the energy along this pathway. It may be seen that the transition state lies 8.5 kcal above the ground state. This compares with the STO-3G barrier height of 5.0 kcal/mol and also the PRDDO barrier height of 2.6 kcal/mol.[28] (In the case of the PRDDO calculation the C_s state is not a transition state but an intermediate 0.2 kcal/mol above the C_{2v} geometry.) The difference in energy between the μ_2-Hückel and *ab initio* transition states is therefore of the same magnitude as the difference between the PRDDO and STO-3G energies. This pathway is confirmed to be a plausible pathway for scrambling of the boron atoms. We compare the *ab initio* and μ_2-Hückel transition state geometries in Figs. 14 and in Table VI. It may be seen that there is reasonable agreement between the Hückel and Hartree–Fock transition state geometries.

As in the B_8H_8 problem, we now turn to a molecular orbital rationalization of this low barrier height. We apply the same interpolation scheme as we did in the $B_8H_8^{2-}$ problem.

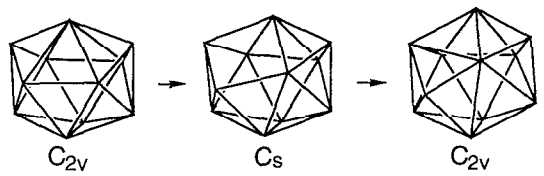

FIG. 15. The dsd pathway for $B_{11}H_{11}^{2-}$.

Unlike the $B_8H_8^{2-}$ system, however it proves to be most convenient to consider the LUMO vs the HOMO. This is so as the $B_{11}H_{11}^{2-}$ system have a number of occupied orbitals of nearly the same energy as the HOMO. As the molecule is generally of C_1 symmetry, these orbitals mix a great deal along the reaction pathway. This orbital mixing generally obfuscates the overall interpolation scheme. In Hückel theory however, calculating the sum of energies of all the unfilled orbitals is equal and opposite to calculating the sum of energies of all the occupied orbitals. In this picture based on holes rather than electrons, it is the LUMO which has the greatest energetic importance. The LUMO of the $B_{11}H_{11}^{2-}$ molecule is fairly separate from other unoccupied orbitals and does not mix well with these other orbitals. The LUMO of the transition state is 4.6 kcal/mol lower in energy than the

TABLE VI. Comparison of RHF and μ_2-Hückel bond distances for $B_{11}H_{11}^{2-}$ ground state and transition state geometries.

Bond	μ_2-Hückel	STO-3G
Ground state geometry (C_{2v})		
a	1.628 (Å)	1.634 (Å)
b	1.766	1.760
c	1.810	1.775
d	1.806	1.847
e	1.570	1.726
f	1.779	1.746
g	1.882	1.822
h	1.809	1.783
i	2.067	1.990
Transition state geometry (C_s)		
a	1.720	1.693
b	1.772	1.775
c	1.562	1.651
d	1.930	1.855
e	1.759	1.801
f	1.958	1.990
g	1.864	1.808
h	1.797	1.751
i	1.665	1.714
j	1.772	1.741
k	1.651	1.596
l	1.776	1.780
m	1.764	1.843
n	1.898	1.820
o	1.754	1.763

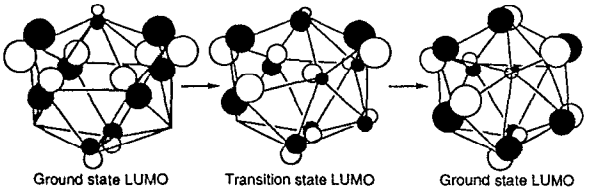

FIG. 17. Evolution of $B_{11}H_{11}^{2-}$ LUMO along the dsd reaction coordinate for $B_{11}H_{11}^{2-}$.

LUMO of the ground state and therefore the change in LUMO energy accounts for slightly over half of the reaction barrier height. In Fig. 17 we illustrate the evolution of the LUMO along the reaction pathway. It may be seen that the transition state LUMO is quite similar to the interpolated average of the two ground state LUMOs. The principal atomic orbitals of the ground state LUMO consist of six p orbitals arranged in a boat-shaped hexagon. These six orbitals are reminiscent of the lowest energy π^* orbital of benzene. This may be contrasted to the LUMO of the transition state which in the view shown in Fig. 17 has on the left-hand side of the molecule a set of four π^* orbitals similar to the most antibonding π orbital in butadiene, and on the right-hand side a relatively isolated p orbital. The average energy of antibonding π^* butadiene orbital and the nonbonded p orbital is roughly equal to that of the ground state LUMO. There is therefore little change in overall LUMO energy across the reaction pathway and hence the reaction is a Woodward–Hoffmann allowed reaction process.

We now turn to the $C_2B_8H_{10}^{2-}$ geometry. The only known geometry of this molecule is a deltahedron with one open hexagonal face.[29] This known structure is illustrated in Fig. 18. In the Williams nomenclature[30] this structure is a nido-10 (vi) cluster (the 10 refers to the number of main group cluster atoms and the roman numeral vi to the number of atoms on the open face). In studying this molecule with μ_2-Hückel theory we found that the global minimum was indeed this nido-10 (vi) geometry illustrated in Fig. 18. However in earlier work[1(i)] with μ_2-Hückel method we found a second energy minimum different from that shown in Fig. 18 which contained an additional C–C bond across the center of the open hexagonal face. It is also illustrated in Fig. 18. In the Williams nomenclature this structure is nido-10 (iv+iv). This isomer (which does not conform with Wade's rules) has subsequently been observed in an isoelectronic nido-10

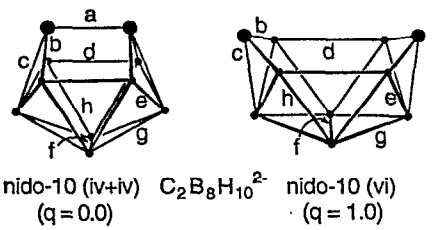

FIG. 18. The nido-10 (iv+iv) and nido-10 (vi) $C_2B_8H_{10}^{2-}$ geometries. Large and small circles represent, respectively, CH and BH units.

TABLE VII. Comparison of bond distances for isomers of $C_2B_8H_{10}^{2-}$.

Bond	μ_2-Hückel[a]	6-31G*	μ_2-Hückel[b]
nido 10 (vi), $q=1$			
b	1.589 (Å)	1.536 (Å)	1.556
c	1.748	1.652	1.619
d	1.927	2.093	1.792
e	1.871	1.858	1.777
f	2.007	2.199	1.894
g	1.829	1.844	1.712
h	1.903	1.842	1.758
nido 10 (iv+iv), $q=0$			
a	1.596 Å	1.556 Å	1.781
b	1.718	1.709	1.778
c	1.798	1.787	1.751
d	1.698	1.717	1.652
e	1.648	1.754	1.631
f	1.740	1.796	1.796
g	1.867	1.808	1.866
h	1.797	1.817	1.697

[a]Standard boron and carbon Hückel parameters were used for the boron and carbon atomic sites.
[b]Boron Hückel parameters were used for carbon atomic sites as well as boron sites.

cluster.[31] We wished to see if this local minimum predicted by μ_2-scaled Hückel theory is also found by *ab initio* methods. We therefore performed RHF calculations at the 6-31G* level. We found that indeed the nido-10 (iv+iv) geometry is a local minimum in *ab initio* theory. We compare bond distances between the *ab initio* and μ_2-scaled Hückel theory for both isomers in Table VII.

In an analogous manner to our earlier study on the disallowed rotation pathway of $B_8H_8^{2-}$ we calculated the energy as a function of a linearly interpolated reaction pathway between the two optimized $C_{2v}C_2B_8H_{10}^{2-}$ geometries, where we set $q=0.0$ and $q=1.0$ to correspond to, respectively, the geometries with and without the central carbon bond. These results are shown in Fig. 19. The *ab initio* and μ_2-scaled

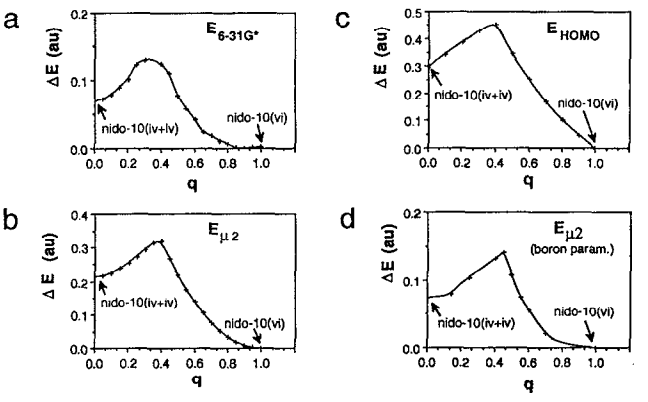

FIG. 19. Energy as a function of distortion coordinate q for $C_2B_8H_{10}^{2-}$ between nido-10 (iv+iv) and nido-10 (vi) geometries using (a) Hartree–Fock 6-31G* energies, (b) μ_2-scaled Hückel theory, (c) HOMO energy of μ_2-scaled Hückel theory, and (d) boron Hückel parameters for both carbon and boron atoms in a μ_2-scaled Hückel calculation. See discussion in the text.

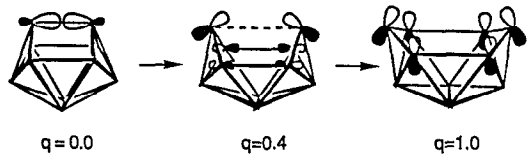

FIG. 20. Principal atomic orbitals in μ_2-Hückel $C_2B_8H_{10}^{2-}$ HOMO.

Hückel theory calculations are in fair qualitative agreement; in both we find a local maximum near the value of $q=0.40$. However the energies of the μ_2-scaled calculations are off by a factor of 2 from the *ab initio* results. None of the previous calculations reported in this paper had errors of this magnitude. In order to examine the source for this discrepancy, we calculated the energy barrier for $B_{10}H_{10}^{4-}$, a molecule isoelectronic with $C_2B_8H_{10}^{2-}$. In the $B_{10}H_{10}^{4-}$ molecule, unlike its carborane counterpart, no heteroatom is severed along the reaction pathway. The overall energetics for this system is illustrated in Fig. 19(d). It can be seen that the μ_2-Hückel calculation for $B_{10}H_{10}^{4-}$ is in much closer agreement with the *ab initio* results. These results suggest that in near-to-covalent systems the actual energetics of a reaction pathway are best modeled by a μ_2-scaled calculation on the isoelectronic homoatomic molecule. As noted earlier, such an approximation breaks down when either ionic or other straight electrostatic interactions play a role in the structure.[32]

We can readily understand the geometric origin of the μ_2-Hückel energies. For this system the total Hückel electronic energy is well modeled by the changes in the HOMO energy alone. In Fig. 19(c) we plot just the energy of this single orbital. It reproduces quite well the full Hückel energy plot of Fig. 19(b). We show the changing form of this HOMO in Fig. 20. At $q=0.0$ the HOMO is predominately carbon–carbon σ bonding. By contrast, the structure at $q=1.0$ is stabilized by allowed mixing of these carbon p orbitals with unoccupied mainly boron orbital of the same symmetry. This mixing changes the HOMO into a carbon to boron π bonding MO. In the intermediate geometry there is neither a strong C–C σ bond nor a C–B π bond. It is for this reason that there is a maximum energy of the value of $q=0.4$.

VII. CONCLUSION

In many ways these last results show succinctly the advantages and disadvantages of the μ_2 scaled technique when compared to *ab initio* theory. One of the advantages is that because the μ_2 method uses Hückel theory we can readily understand on a qualitative level the precise electronic factors which influence the total energy. A second advantage is that μ_2-Hückel theory can be carried out quickly and at low cost. This low cost allows one a great latitude in the number of geometries one chooses to study. Our results for $C_2B_8H_{10}^{2-}$ suggest that μ_2-Hückel theory can be used to find potential new isomers which can then be explicitly tested at a more accurate *ab initio* level. The disadvantage of the μ_2-Hückel theory is its incomplete modeling of the various factors which control the electronic energy. For example, μ_2-Hückel theory does not as yet contain terms which model the relation between charge transfer or ionic energies and structure. This limits the applications of the method for noncovalent systems. We believe that in the end a combination of both approaches leads to the clearest picture of the bonding in the boranes as well as other covalent and nearly covalent compounds. Hartree–Fock calculations will allow the chemist to assess the full electronic energy. By contrast μ_2-Hückel theory will let one measure the pure covalent forces. It in turn will form a bridge to such qualitative molecular orbital ideas such as the fragment formalism, symmetry analysis, and the isolobal analogy. With these tools the chemist can form a vivid and accurate picture of the bonding in both molecules and solids.

ACKNOWLEDGMENTS

This research was supported by funds from the Petroleum Research Fund. The research would not have been possible without the computer programs developed by R. Hoffmann, M.-H. Whangbo, M. Evain, T. Hughbanks, S. Wijeyesekera, M. Kertesz, C. N. Wilker, C. Zheng, J. K. Burdett, and G. Miller. We thank the National Science and Engineering Research Council of Canada for a research fellowship granted to R. R. and the Alfred P. Sloan Foundation and the John D. and Catherine T. MacArthur Foundation for fellowships granted to S. L. We thank Cyndi Wells and Greg Grieves for their help with the $B_{11}H_{11}^{2-}$ reaction pathway.

[1] (a) W. M. Hehre, L. Radom, P. V. R. Schleyer, and J. A. Pople, *Ab Initio Molecular Orbital Theory* (Wiley–Interscience, New York, 1986); and (b) J. Hafner, *From Hamiltonians to Phase Diagrams* (Springer, New York, 1987); (c) A. Szabo, and N. S. Ostlund, *Modern Quantum Chemistry* (McGraw–Hill, New York, 1982).

[2] (a) R. Hoffmann, J. Chem. Phys. **39**, 1397 (1963); (b) R. B. Woodward and R. Hoffmann, *The Conservation of Orbital Symmetry* (VCH, New York, 1970); (c) T. A. Albright, J. K. Burdett, and M. H. Whangbo, *Orbital Interactions in Chemistry* (Wiley, New York, 1985); (d) N. L. Allinger, Molecular Mechanics Int. Union Crystallogr. Monogr. Crystallogr. **1**, 336 (1992).

[3] (a) D. G. Pettifor and R. Podloucky, Phys. Rev. Lett. **53**, 1080 (1984); (b) J. K. Burdett and S. Lee, J. Am. Chem. Soc. **107**, 3063 (1985); (c) D. G. Pettifor, J. Phys. C **19**, 285 (1986); (d) J. C. Cressoni and D. G. Pettifor, J. Phys. **3**, 495 (1991); (e) S. Lee, J. Am. Chem. Soc. **113**, 101, 8611 (1991); (f) L. M. Hoistad, S. Lee, and J. Paternak, *ibid.* **114**, 4790 (1992); (g) L. M. Hoistad and S. Lee, *ibid.* **113**, 8216 (1991); (h) S. Lee, Acc. Chem. Res. **24**, 249 (1991); (i) Inorg. Chem. **16**, 651 (1992); (j) S. Lee, R. Rousseau, and C. Wells, Phys. Rev. B **46**, 12 121 (1992); (k) S. Lee and B. Foran, J. Am. Chem. Soc. **116**, 154 (1994).

[4] (a) K. Wade, Adv. Inorg. Chem. Radiochem. **18**, 1 (1976); (b) R. W. Rudolph and W. R. Pretzer, Inorg. Chem. **11**, 1974 (1972); (c) R. E. Williams, *ibid.* **11**, 210 (1971); (d) A. J. Stone, *ibid.* **20**, 563 (1981); (e) D. M. P. Mingos, Acc. Chem. Res. **17**, 311 (1984); (f) W. N. Lipscomb, *Boron Hydrides* (Benjamin, New York, 1963); (g) E. L. Muetterties and W. H. Knoth, *Polyhedral Boranes* (Wiley, New York, 1968).

[5] (a) W. Hume-Rothery and G. V. Raynor, *The Structure of Metals and Alloys* (Institute of Metal, London, 1962); (b) W. Hume-Rothery, in *Phase Stability in Metals and Alloys*, edited by P. S. Rudman, J. Stringer, and R. I. Jaffee (McGraw-Hill, New York, 1976), p. 3.

[6] (a) For a description of the elemental structures see J. Donohue, *The Structure of the Elements* (Wiley, New York, 1974); (b) $LaSe_2$: S. Bénazeth, D. Carré, and P. Laruelle, Acta Crystallogr. B **38**, 33 (1982); (d) $La_{10}Se_{19}$: M. Grupe and W. Urland, J. Less. Common. Metals **170**, 271 (1991); (e) $RbDy_3Se_8$: B. Foran, S. Lee, and M. Aronson, Chem. Mater. **5**, 974 (1993); (f) For molecular structures see references in Ref. 3(f).

[7] For a discussion of the effect of changes in coordination number on Hückel electronic energies see J. K. Burdett, Struct. Bond. **65**, 29 (1987).

The effect of this coordination number problem for the Hückel theory of boranes is well studied in (a) W. W. Porterfield, M. E. Jones, W. R. Gill and K. Wade, Inorg. Chem. **29**, 2914 (1990); (b) W. W. Porterfield, M. E. Jones, and K. Wade, *ibid.* **29**, 2919, 2923, and 2927 (1990).

[8] G. Herzberg, *Molecular Spectra and Molecular Structure: Spectra of Diatomic Molecules* (Van Nostrand, Princeton, NJ, 1950).

[9] (a) R. S. Mulliken, C. A. Rieke, D. Orloff, and H. Orloff, J. Chem. Phys. **17**, 1278 (1949); (b) C. C. J. Roothan, *ibid.* **19**, 1443 (1951).

[10] M. Wolfsberg and L. Helmholz, J. Chem. Phys. **20**, 83 (1957).

[11] V. Heine, I. J. Robertson, and M. G. Payne, Philos. Trans. R. Soc. London Ser. A **334**, 393 (1991).

[12] Many important atomic parameters are used and discussed in (a) R. Hoffmann, J. Chem. Phys. **39**, 1397 (1963); A. B. Anderson and R. Hoffmann, *ibid.* **60**, 4271 (1974); (b) A. R. Rossi and R. Hoffmann, Inorg. Chem. **14**, 365 (1975); (c) P. J. Hay, J. C. Thibeault, and R. Hoffmann, J. Am. Chem. Soc. **97**, 4884 (1975); (d) M. Elian and R. Hoffmann, Inorg. Chem. **14**, 1058 (1975); (e) R. H. Summerville and R. J. Hoffmann, J. Am. Chem. Soc. **98**, 7240 (1976); (f) J. W. Lauher and R. Hoffmann, *ibid.* **98**, 1729 (1976); (g) S. Komiya, T. A. Albright, and R. Hoffmann, Inorg. Chem. **17**, 126 (1978); (h) T. Hughbanks, R. Hoffmann, M.-H. Whangbo, K. Stewart, O. Einstein, and E. Canadell, J. Am. Chem. Soc. **104**, 3876 (1982); (i) D. Thorn and R. Hoffmann, Inorg. Chem. **17**, 126 (1978).

[13] (a) E. Clementi and C. Roetti, At. Data Nucl. Data Tables **14**, 177 (1974); (b) J. B. Mann, *Atomic Structures Calculations, 1: Hartree-Fock Energy Results for Elements Hydrogen to Lawrencium* (Clearinghouse for Tech. Lit., Springfield, 1967).

[14] (a) $B_8H_8^{2-}$: L. Guggenberger, J. Inorg. Chem. **8**, 2771 (1969); (b) $B_9H_9^{2-}$: **7**, 2261 (1968); (c) $B_{10}H_{10}^{2-}$: J. T. Gill and S. Lippard, *ibid.* **14**, 751 (1975).

[15] Recent *ab initio* calculations on borohydrides include: (a) M. Buehl and P. Von R. Schleyer, *In Electron Deficient Boron and Carbon Clusters*, edited by G. A. Olah, K. Wade, and R. E. Williams (Wiley, New York, 1991), p. 113; (b) M. L. McKee, J. Am. Chem. Soc. **114**, 879 (1992); (c) M. Bühl and P. v. R. Schleyer, *ibid.* **114**, 477 (1992); (d) M. L. McKee, *ibid.* **113**, 9448 (1991); (e) A. M. Mebel, O. P. Charkin, M. Bühl, and P. v. R. Schleyer, Inorg. Chem. **32**, 463 (1993); (f) M. L. McKee, M. Bühl, and P. v. R. Schleyer, *ibid.* **32**, 1712 (1993); (g) A. M. Mebel, O. P. Charkin, and P. v. R. Schleyer, *ibid.* **32**, 469 (1993).

[16] In this article all the reported Hartree–Fock calculations used the Gaussian 90 molecular orbital package (Gaussian 90 Revision 1; M. J. Frisch, M. Head-Gordon, G. W. Tucks, J. B. Foresman, H. B. Schelegel, K. Raghavachari, M. Robb, J. S. Binkley, C. Gonzalez, D. J. Fox, R. A. Whiteside, R. Seager, C. F. Melius, J. Baker, R. L. Martin, L. R. Kahn, S. Topoil, and J. A. Pople, Gaussian Inc. Pittsburgh, PA, 1990).

[17] We have studied the effect of point group symmetry on the electronic energy of borohydride clusters in Ref. 3(f).

[18] Characterization of all stationary points on the potential energy surface was conducted by calculation of theoretical vibrational spectra. For the μ_2-Hückel surface, a Hessian matrix was calculated numerically for the $3N$ mass weighed Cartesian coordinates of the N skeletal boron or carbon atoms of the clusters. Rotational, translational and one coordinate corresponding to size expansion (not a variable in second moment scaled Hückel theory) were subtracted from the vibrational spectrum prior to stationary point characterization. Thus, in μ_2-Hückel theory there are $3N-7$ relevant of internal motion for clusters of this type. This compares to the $3n-6$ (where n is the total number of atoms in the cluster) degrees associated with the *ab initio* calculations. Note that in closo-systems $n=2N$ as there are equal numbers of hydrogen and boron atoms. Thus we see that frequencies derived from μ_2-Hückel theory cannot be quantitatively compared to Hartree–Fock calculations. We therefore cannot use μ_2-Hückel theory for vibrational analysis studies.

[19] The parameters used for Hückel calculations correspond to those compiled in Ref. 12. For carbon the parameters are $H_{ii}(2s)=-21.4$ eV, $H_{ii}(2p)=-11.4$ eV, $\zeta(2s)=1.625$, and $\zeta(2p)=1.625$. For hydrogen the parameters are $H_{ii}(1s)=-13.6$ eV and $\zeta(1s)=1.30$. Boron parameters are given in the text.

[20] For this detailed analysis using the Walsh diagram approach see R. Rousseau, and S. Lee, in *Graph Theory Approaches to Chemical Reactivity*, edited by D. Bonchev (Kluwer, Dordrecht, in press).

[21] At $\theta=51°$ the bond lengths are $a=1.46$ Å, $b=2.13$ Å, and $c=2.32$ Å as compared to $\theta=60°$, $a=1.68$ Å, $b=1.79$ Å, $c=1.87$ Å.

[22] (a) E. L. Muetterties, R. J. Wiersema, and M. F. Hawthorne, J. Am. Chem. Soc. **95**, 7520 (1973); (b) E. L. Muetterties, Tetrahedron **30**, 1595 (1974).

[23] (a) W. N. Lipscomb, Science **153**, 373 (1966); (b) D. P. M. Mingos and D. J. Wales, in *Electron Deficient Boron and Carbon Clusters*, edited by G. A. Olah, K. Wade, and R. E. Williams (Wiley, New York, 1991); (c) A. Rodgers and B. F. G. Johnson, Polyhedron **7**, 1107 (1988); (d) R. B. King, Inorg. Chim. Acta **49**, 237 (1981); Theor. Chem. Acta **64**, 439 (1984); (e) D. J. Wales, D. M. P. Mingos, and Z. Lin, Inorg. Chem. **28**, 2754 (1989).

[24] (a) D. A. Kleier and W. N. Lipscomb, Inorg. Chem. **18**, 1312 (1979); (b) D. J. Wales and R. G. A. Bone, J. Am. Chem. Soc. **114**, 5394 (1992); (c) J. W. Bausch, G. K. Surga Prakash, and R. E. Williams, Inorg. Chem. **31**, 3763 (1992); (d) M. Bühl, A. M. Mebel, O. P. Charkin, and P. v. R. Schleyer, *ibid.* **31**, 3769 (1992); (e) D. J. Wales, J. Am. Chem. Soc. **115**, 11 191 (1993); (f) D. J. Wales and A. J. Stone, Inorg. Chem. **26**, 3845 (1987).

[25] (a) K. Müller and L. D. Brown, Theor. Chem. Acta **53**, 77 (1979); (b) M. J. S. Dewar, E. F. Healey, and J. P. Stewart, J. Chem. Soc. Faraday Trans. 2 **80**, 272 (1989).

[26] A detailed analysis of other diamond to square to diamond rearrangements for closo $B_nH_n^{2-}$ clusters exists in the literature. It is known that $B_8H_8^{2-}$ and $B_{11}H_{11}^{2-}$ are Woodward–Hoffmann allowed processes and that they are fluxional. By contrast in $B_5H_5^{2-}$ and $B_9H_9^{2-}$ the diamond to square to diamond rearrangements are symmetry disallowed processes and the molecules are not fluxional. See B. M. Gimarc and J. J. Ott, Inorg. Chem. **25**, 83, 2708 (1986).

[27] (a) E. I. Tolpin and W. N. Lipscomb, J. Am. Chem. Soc. **95**, 2384 (1973); (b) E. L. Muetteries, E. L. Hoel, C. G. Salentine, and M. F. Hawthorne, Inorg. Chem. **14**, 950 (1975).

[28] (a) D. A. Kleier, D. A. Dixon, and W. N. Lipscomb, Inorg. Chem. **17**, 166 (1978); (b) B. M. Gimarc, B. Dai, D. S. Warren, and J. J. Ott, J. Am. Chem. Soc. **112**, 2597 (1990).

[29] B. Stibr, Z. Janousek, K. Base, S. Hermanek, J. Plesek, and I. Zakharova, Collect. Czech. Chem. Commun. **49**, 1891 (1984).

[30] R. E. Williams, in *Electron Defficient Boron and Carbon Clusters*, edited by G. A. Olah, K. E. Wade, and R. E. Williams (Wiley, New York, 1991).

[31] C. Scott, B. W. Eichhorn, and S. G. Bott, J. Am. Chem. Soc. **115**, 5837 (1993).

[32] It is important to note that the isoelectronic homoatomic Hückel calculation neglects any effects of the overall increase in the total net charge of the system. It is clear that in a -4 cluster, this net charge should have an important consequence. At the *ab initio* 3-21G* level for instance, calculations show that neither $B_{10}H_{10}^{4-}$ nor $Li_2[B_{10}H_{10}^{4-}]$ have a stable nido-10 (iv+iv) isomer.